

Anticounterfeiting Labels with Smartphone-Readable Dynamic Luminescent Patterns Based on Tailored Persistent Lifetimes in $\text{Gd}_2\text{O}_2\text{S}:\text{Eu}^{3+}/\text{Ti}^{4+}$

Ngei Katumo, Luis Arturo Ruiz-Preciado, Vinay Kumar, Gerardo Hernandez-Sosa, Bryce S. Richards, and Ian A. Howard*

Dynamic luminescent labels, in which a luminescent image changes with time after ultraviolet excitation is turned off, are attractive for anticounterfeiting. A sequence of $\text{Gd}_2\text{O}_2\text{S}:\text{Eu}^{3+}/\text{Ti}^{4+}$ phosphors is presented in which the Ti^{4+} doping concentration allows the persistent emission lifetime to be varied from 1.17 ± 0.02 to 5.95 ± 0.07 s. While this persistent lifetime is tuned, the photoluminescence quantum yield remains over $46\% \pm 3\%$. A broad charge-transfer band allows these phosphors to be excited with inexpensive and relatively safe 375 nm light-emitting diodes. By developing patterns with phosphors that have differing persistent lifetimes, dynamic changes in the luminescent image after the excitation source is removed can be observed. For patterns made from phosphor materials that have big differences in persistent lifetimes, these dynamic changes are observable by the eye. By contrast, the dynamic changes in patterns made by phosphors with comparable persistent lifetimes (0.20 s delayed lifetime difference) are difficult to observe by the naked eye but can be easily determined by analysis of a 30-frames-per-second video taken with a smartphone. Thus, these bright phosphors with tunable persistent lifetime allow both overt (observable by eye) and covert (requiring smartphone video analysis) dynamic anticounterfeiting labels to be created.

1. Introduction

The production of counterfeit goods and the forging of currencies and documents create both financial and safety-related problems for manufacturers and governments. In the period 2008 to 2013, the global economic loss due to counterfeiting increased fivefold from USD 200 billion to USD 1.13 trillion and is projected to reach USD 2.81 trillion by 2022.^[1] This significant and increasing loss due to fakes introduces opportunities for more effective anticounterfeiting measures; the implementation of technologies designed to make products harder to copy or make it easier to distinguish genuine products from fake ones. The latter usually involves marking the product with a difficult-to-replicate label. Examples of such anticounterfeiting labels include digital and smart signatures,^[2] plasmonic labels,^[3] magnetic tags,^[4] holograms,^[5] physical-unclonable-functions,^[6] and luminescence

tags.^[7] Luminescence tags are of particular interest for preventing counterfeiting due to their unique and tunable optical properties, ease of adoption and integration with other anticounterfeiting technologies.

In the field of luminescence tags, the first approach is to create security images invisible under standard conditions but revealed under the appropriate illumination. Work by Andres et al. demonstrated full-color images using lanthanide-based inks under ultraviolet (UV) illumination, which are invisible in the absence of the excitation source.^[7a] Such an approach can be extended by also requiring correct environmental conditions for the luminescence to be visible. For example, Zhao et al. present interesting anticounterfeiting features reliant on thermo-hydro-chromic properties of oxazolidines and hydrochromic molecules for emission-based dual encryption.^[8] They demonstrated that changing either the moisture content or temperature of their labels revealed the coded information. To secure luminescent labels beyond a simple response to UV light, recent strategies include multi-mode emissions,^[9] dual-mode excitation color tuning,^[10] external stimuli-coded luminescence,^[2b] dynamic photoluminescence,^[11] and integrated time-resolved luminescence.^[12]

N. Katumo, V. Kumar, Dr. G. Hernandez-Sosa, Prof. B. S. Richards, Dr. I. A. Howard
Institute of Microstructure Technology
Karlsruhe Institute of Technology
Hermann-von-Helmholtz-Platz 1
76344 Eggenstein-Leopoldshafen, Germany
E-mail: ian.howard@kit.edu

L. A. Ruiz-Preciado, Dr. G. Hernandez-Sosa, Prof. B. S. Richards, Dr. I. A. Howard
Light Technology Institute
Karlsruhe Institute of Technology
Engesserstrasse 13, 76131 Karlsruhe, Germany

L. A. Ruiz-Preciado, Dr. G. Hernandez-Sosa
InnovationLab
Speyerer Strasse 4, 69115 Heidelberg, Germany

 The ORCID identification number(s) for the author(s) of this article can be found under <https://doi.org/10.1002/admt.202100047>.

© 2021 The Authors. Advanced Materials Technologies published by Wiley-VCH GmbH. This is an open access article under the terms of the Creative Commons Attribution-NonCommercial License, which permits use, distribution and reproduction in any medium, provided the original work is properly cited and is not used for commercial purposes.

DOI: 10.1002/admt.202100047

Another potential strategy to increase the security of luminescent labels involves uniquely identifying labels based on determining the lifetime(s) of the luminescence of various parts of the label. Typically, these luminescence lifetimes are shorter than a few milliseconds, and therefore need dedicated equipment to resolve their lifetime. For example, the work of Lu et al. focused on the development of lifetime-based multiplexing nanocrystals in the 26 to 662 μ s range for advanced encryption and coding but required a scanning microscope to read out the photoluminescence (PL) lifetime.^[12d] Sun et al. used nanosecond range PL lifetimes of iridium (III) complexes as smart luminescent materials for data recording and security applications, but this approach also needs a fluorescence lifetime imaging microscopy setup to authenticate.^[13] Kalytchuk et al. reported the use of carbon dot fluorescence-lifetime for anticounterfeit applications, which also relied on single-photon counting-based fluorescence imaging to decode the PL lifetimes.^[14] Recent elegant work by Ding et al. demonstrates how oxygen-sensitive organic chromophores can be inkjet printed to make labels whose three levels of security rely on the combination of dynamic lifetime-based imaging and tailored environmental response.^[15] With lifetimes varying from 10 to 100 μ s, an ICCD camera is still needed to image these short lifetimes.

Delayed luminescence materials with lifetimes in the range of seconds to hours can be used to move the concept of PL lifetime-based anticounterfeiting into a regime where the human eye can be used to discern the changing PL pattern after excitation stops. Many inorganic persistent phosphors, wherein charge carriers are trapped under UV illumination and delayed luminescence occurs after the illumination ceases due to thermal detrapping of the charges, have been developed.^[16] The most ubiquitous, commonly used in emergency signs, is $\text{SrAl}_2\text{O}_4:\text{Eu}^{2+}:\text{Dy}^{3+}$ with a lifetime exceeding tens of hours.^[16] Ji et al. recently demonstrated the potential of the persistent phosphor $\text{Sr}_2\text{Ga}_2\text{GeO}_7:\text{Pr}^{3+}$ for dynamic anticounterfeiting.^[9e] Changing the Pr^{3+} doping from 0.2% to 3.0% significantly decreased the persistence lifetime and allowed a clear difference in the emission pattern of a printed label observed 90 and 300 s after excitation at 254 nm. Pei and co-workers similarly showed dynamic anticounterfeiting based on $\text{NaCa}_2\text{GeO}_4:\text{F}:\text{Tb}^{3+}$ with the persistent luminescence color and lifetime after 254 nm excitation altered by Tb^{3+} concentration.^[17] Long et al. designed quasi-layer structured $\text{Ca}_3\text{Ga}_4\text{O}_9:\text{Bi}^{3+}$ to show persistent luminescence alongside photostimulated luminescence, and variation of the prompt PL color for a strong anticounterfeiting material, again using 254 nm excitation for persistent luminescence.^[18] Similarly, Sang and co-workers combined persistent luminescence and mechanoluminescence in niobate structures for anticounterfeiting.^[19] Organic materials can also show delayed luminescence suitable for dynamic anticounterfeiting by mechanisms including room-temperature phosphorescence,^[20] and emission from states with a strong charge-transfer character.^[19,21] Also, carbon dots can show delayed luminescence useful for anticounterfeiting.^[22] However, to move beyond the analysis of dynamic counterfeiting labels by eye, it would be desirable to have a sequence of persistent phosphors that allow a standard camera, such as that found

in a smartphone, to perform quantitative lifetime-based image analysis. In this contribution, we develop such a sequence of easily excitable and uniformly bright persistent phosphors whose persistent lifetimes can be precisely controlled. These enable anticounterfeiting security through an overt analysis by eye and covert quantitative lifetime analysis based on videos shot with a smartphone camera.

The desired delayed lifetime range of the ideal phosphors for smartphone-based lifetime determination can be considered as follows. The lower limit is imposed by the frame rate of the camera, its sensitivity, and the intensity of the emission. With the standard 30 frames-per-second (fps) camera found in a smartphone, we previously demonstrated that persistent lifetimes longer than 100 ms can be determined by examining the temperature-dependent PL lifetime of $\text{Gd}_2\text{O}_2\text{S}:\text{Eu}^{3+}$.^[23] The upper limit on the persistent lifetime is a practical consideration of how long an authentication measurement can take for a given application. For point-of-sale authentication by consumers, we approximate that the authentication time should stay under 10 s, and therefore that the decay time of the phosphor should be shorter than a few seconds. For persistent lifetimes in this regime, there are few inorganic material systems doped with lanthanide emitters that can demonstrate bright delayed lifetimes within this window. Choices include the oxysulphides,^[24] aluminates,^[25] and alkali earth (Ca, Sr, and Ba) silicate oxides.^[9e,11a,26]

We have previously demonstrated that $\text{Gd}_2\text{O}_2\text{S}:\text{Eu}^{3+}$ exhibits a bright delayed emission whose persistent lifetime can easily be established from a video captured with a smartphone camera.^[23] The $\text{Gd}_2\text{O}_2\text{S}:\text{Eu}^{3+}$ host also has the advantage that it has a broad charge-transfer band (CTB) that can be excited by 375 nm LEDs. This 375 nm UVA excitation wavelength is more attractive than the UVC (254 nm) normally needed for host absorption because 1) the light-emitting diodes (LEDs) are tenfold less expensive, 2) are on average tenfold brighter (higher external quantum efficiency),^[27] and 3) the UVA emission is much less hazardous for the skin and eyes.^[28] In our previous study, the variation of the persistent lifetime with temperature allowed the material to be applied for optical thermography.^[23] However, given only a single persistent lifetime is accessible at a certain temperature, it is not applicable for anticounterfeiting. In this contribution, we report how the persistent lifetime of the bright delayed emission in this material can be varied based on Ti^{4+} codoping, allowing phosphors with varying persistent lifetimes to be developed for anticounterfeiting purposes. We demonstrate prototype labels based on patterns of $\text{Gd}_2\text{O}_2\text{S}:\text{Eu}^{3+}/\text{Ti}^{4+}$ phosphors with varying persistent lifetimes and demonstrate how the labels can be authenticated either by eye or with the assistance of a smartphone video.

2. Results and Discussion

First, we explored the structural properties and morphology of the oxysulphide $\text{Gd}_2\text{O}_2\text{S}:\text{6\% Eu}^{3+}/x\% \text{Ti}^{4+}$ phosphors as a function of the Ti^{4+} codoping (ranging from $x = 0$ to 24 mol%) by undertaking X-ray diffraction (XRD) analysis and imaging using a scanning electron microscope (SEM). The XRD

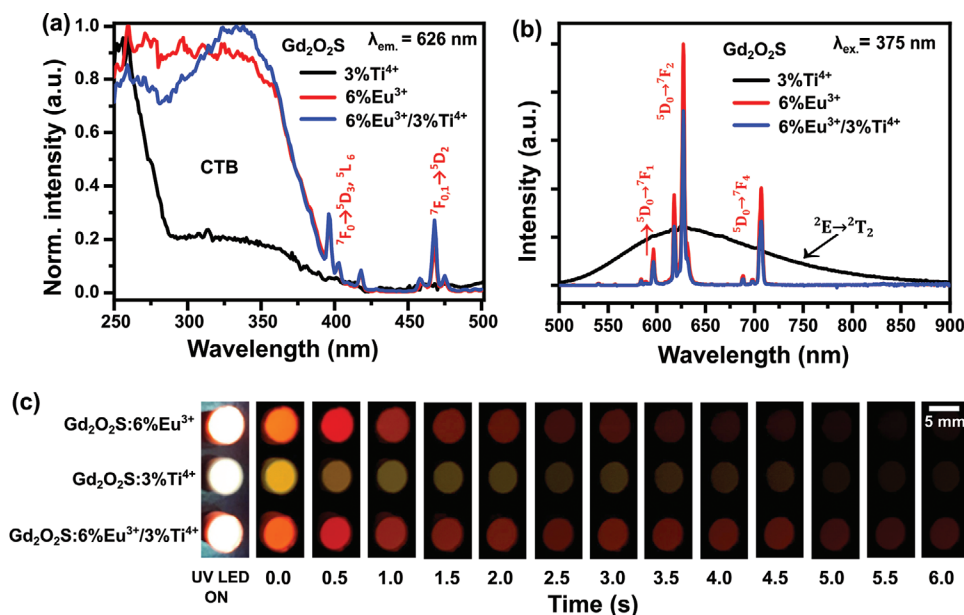


Figure 1. a) PL excitation spectra for Gd₂O₂S:3%Ti⁴⁺, Gd₂O₂S:6%Eu³⁺, and Gd₂O₂S:6%Eu³⁺/3%Ti⁴⁺ (tracking the emission at $\lambda_{em} = 626$ nm). The spectrum consists of a broad CTB in the 250–400 nm range and sharp bands common in Eu³⁺ intraconfigurational transitions. The CTB of Gd₂O₂S:3%Ti⁴⁺ is relatively weak, with absorption peaking in the 250–290 nm region. The observed bands include the ${}^7F_{0,1} \rightarrow {}^5D_3, {}^5L_6$ (396–417 nm), and ${}^7F_{0,1} \rightarrow {}^7D_2$ (468 nm) Eu³⁺ transitions. b) PL emission spectra of Gd₂O₂S:3%Ti⁴⁺, Gd₂O₂S:6%Eu³⁺, and Gd₂O₂S:6%Eu³⁺/3%Ti⁴⁺ under 375 nm excitation at room temperature. The emission spectra of Gd₂O₂S:6%Eu³⁺ and Gd₂O₂S:6%Eu³⁺/3%Ti⁴⁺ consists of ${}^5D_0 \rightarrow {}^7F_j$ (for $j = 0, 1, 2,$ and 4) Eu³⁺ transitions with a dominant emission being the ${}^5D_0 \rightarrow {}^7F_2$ (626 nm) with a left shoulder at 616 nm, while the PL emission of Gd₂O₂S:3%Ti⁴⁺ exhibits a broadband emission. c) Video frames extracted from videos of luminescence of Gd₂O₂S: 6%Eu³⁺, Gd₂O₂S:3%Ti⁴⁺, and Gd₂O₂S:6%Eu³⁺/3%Ti⁴⁺ after excitation under $\lambda_{ex} = 375$ nm showing the afterglow characteristics of the three samples as a function of time.

patterns and the SEM images are as shown in Figures S1 and S2 respectively in the Supporting Information. The XRD patterns revealed that the phosphors had a trigonal structure, space group $P-3m1(164)$, and were mapped to ICSD 167755. At higher Ti⁴⁺ codoping (more than 12 Ti mol%), traces of Gd₂Ti₂O₇ that were mapped to ICSD 167918 were observed. The SEM images revealed that the phosphors had quasi-spherical morphology, loosely clustered, and with a distributed particle size in the range of 0.2–5 μ m.

The PL excitation and emission spectra of the Gd₂O₂S micro-phosphors with various doping concentrations are plotted in Figure 1. As observed in the PL excitation spectra (tracking the 626 nm emission) in Figure 1a, both Gd₂O₂S:6%Eu³⁺ and Gd₂O₂S:6%Eu³⁺/3%Ti⁴⁺ shows a strong CTB, in the 250–400 nm region. This strong CTB in Gd₂O₂S:6%Eu³⁺ and Gd₂O₂S:6%Eu³⁺/3%Ti⁴⁺ is mainly due to charge transfer between S²⁻/O²⁻ and Eu³⁺ [29] and only weakly affected by the O²⁻ to Tiⁿ⁺ ($n = 3, 4$) charge transfer. [30] The other absorption bands include the Eu³⁺ intraconfigurational transitions ${}^7F_{0,1} \rightarrow {}^5D_3, {}^5L_6$ (396–418 nm) and ${}^7F_{0,1} \rightarrow {}^7D_2$ (468 nm). [29a,b,31] The Gd₂O₂S:3%Ti⁴⁺ PL excitation spectrum, tracked from its emission peak at 626 nm, peaking in the UVC region (260 nm) coinciding with 4.8 eV bandgap of the undoped host material, and shows a weak CTB roughly in the same place Gd₂O₂S:6%Eu³⁺. [29c] The broad CTB, dominated by the Eu³⁺ CTB, allows the cheaper and safer UVA excitation with a 375 nm LED. Additional information on the PL excitation spectra of the other Gd₂O₂S:6%Eu³⁺/ x %Ti⁴⁺ can be found in Figure S4 of the Supporting Information.

The PL emission spectra of Gd₂O₂S:6%Eu³⁺, Gd₂O₂S:3%Ti⁴⁺, and Gd₂O₂S:6%Eu³⁺/3%Ti⁴⁺ under 375 nm LED excitation are displayed in Figure 1b. The PL emission spectra of Gd₂O₂S:3%Ti⁴⁺ exhibits a broad emission band in the 500–900 nm region, peaking at 626 nm due to the Ti³⁺ (${}^2E \rightarrow {}^2T_2$) transition. [32] This is consistent with previous reports on Ti⁴⁺ emission in oxysulphide hosts, where the excited Ti⁴⁺ ion quickly captures an electron forming an excited Ti³⁺* ion that then combines with a hole leading to the observed emission. [32,33] The Gd₂O₂S:6%Eu³⁺ and Gd₂O₂S:6%Eu³⁺/3%Ti⁴⁺ displayed the typical Eu³⁺ emission spectra with no trace of emission from Ti (neither in the prompt emission in Figure 1b nor in the delayed emission in Figure S7, Supporting Information). The main emission peak in both cases was the ${}^5D_0 \rightarrow {}^7F_2$ (626 nm) Eu³⁺ transition that had a shoulder at 617 nm. The other transitions include the ${}^5D_0 \rightarrow {}^7F_{0,1}$ (596 nm), and ${}^5D_0 \rightarrow {}^7F_4$ (704 nm). Maintaining the narrowband emission from the Eu³⁺ for both the prompt and delayed luminescence is highly desirable because the high spectral brightness of this narrowband emission is attractive for distinguished it from ambient lighting using bandpass filters. [23] Note that the narrowband emission from Eu is not maintained in all hosts codoped with Ti⁴⁺. For example, in Y₂O₂S:Eu³⁺/Ti⁴⁺/Mg²⁺, the broad emission from the Ti is clearly visible in the delayed emission. [34] The mechanism will be discussed in detail later, but these results indicate electron transfer from the Ti³⁺ to the Eu²⁺ in our host, which is absent in Y₂O₂S. This transfer of the electron from Ti to Eu in the Gd₂O₂S, but not in the Y₂O₂S is consistent with the smaller difference in the vacuum referenced binding energies for Eu

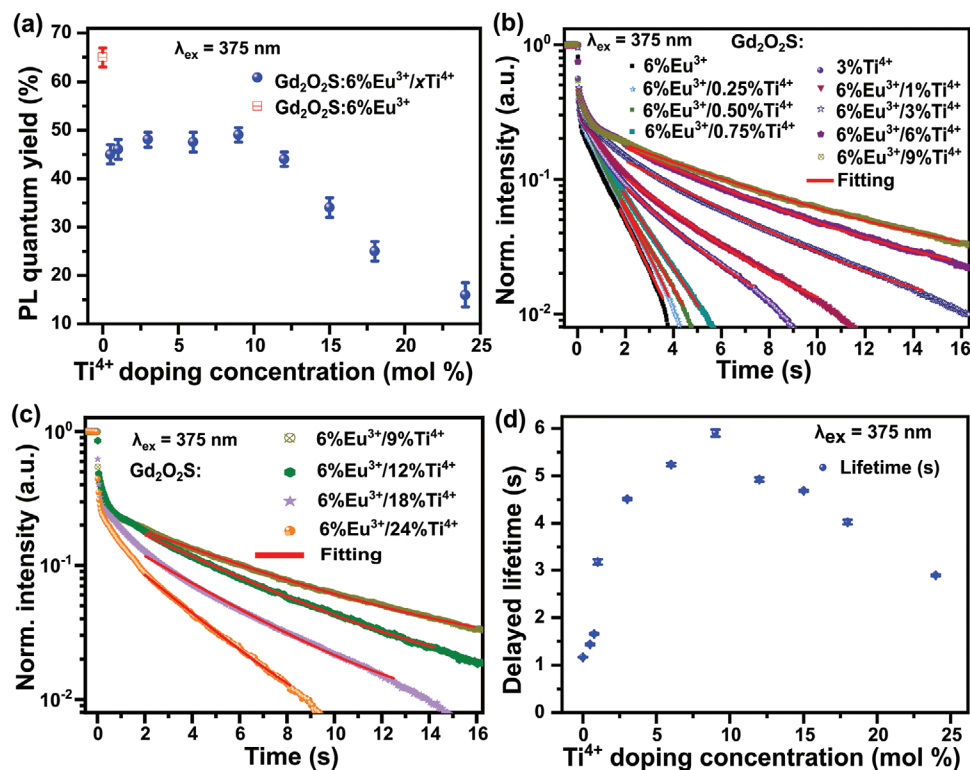


Figure 2. a) Measured absolute PLQY values of the Gd₂O₂S:6%Eu³⁺/xTi⁴⁺ phosphors for (0 < x < 24% mol) under λ_{ex} = 375 nm excitation. The Ti⁴⁺ codoping first leads to relatively constant PLQY followed by a steady decrease beyond 9% Ti⁴⁺ codoping. b) Normalized delayed emission intensity as a function of time extracted from smartphone-acquired videos of Gd₂O₂S:6%Eu³⁺/x%Ti⁴⁺ emissions after pulsed UV-LED excitation (375 nm), for lower Ti⁴⁺ concentrations (x = 0, 1, 3, 6, and 9 mol%) and for c) higher Ti⁴⁺ concentrations (x = 9, 12, 18, and 24% mol). d) The delayed lifetime (τ) from a single exponential fitting $y = y_0 + A_1 \exp(-t/\tau)$ in the delayed PL region of interest for each case. The delayed PL lifetime can be tuned to be within the range of 1.17 ± 0.02 to 5.95 ± 0.07 s with the lifetimes increasing up to 9% Ti⁴⁺ codoping and then decreases with further increase in Ti⁴⁺ codoping.

and Ti in the Gd₂O₂S host recently established in the literature.^[35] The mechanistic understanding is discussed in more detail later.

In our previous work, we optimized the photoluminescence quantum yield (PLQY) of Gd₂O₂S:x% Eu³⁺ (ranging from x = 0 to 13 mol%) doping, with 6% Eu³⁺ doping registering the best PLQY of 65% (λ_{ex} = 375 nm).^[23] Therefore, this work is based on Ti⁴⁺ codoping of the Gd₂O₂S:6% Eu³⁺ optimized phosphors. Figure 1c displays smartphone-video-recorded delayed luminescence of Gd₂O₂S:6%Eu³⁺, Gd₂O₂S:3%Ti⁴⁺, and Gd₂O₂S:6%Eu³⁺/3%Ti⁴⁺ upon 375 nm UV excitation for 10 s. The Gd₂O₂S:6%Eu³⁺ exhibit a short, delayed PL emission with the afterglow being observable up to for ≈4 s after the 375 nm LED excitation is switched off. Alternatively, the Gd₂O₂S:3%Ti⁴⁺ has a longer delayed PL emission, which is observable beyond 6 s despite having a low PL intensity. The Gd₂O₂S:6%Eu³⁺/3%Ti⁴⁺ synergistically demonstrates both high PL emission and longer delayed lifetime.

A sequence of Gd₂O₂S:6% Eu³⁺ phosphors was synthesized in which the codoping of the Ti⁴⁺ ions was varied between 1 and 24 mol%. The PLQY and delayed lifetime as a function of Ti⁴⁺ codoping concentration is presented in Figure 2. The steady-state PLQY without Ti⁴⁺ codoping is 65%. The PLQY reduces to 46% ± 3% for Ti⁴⁺ concentrations from 0.25 and 9 mol% but remains constant at this reasonably high level throughout

this range (Figure 2a). While the PLQY remained similar for the range under 9 mol% Ti⁴⁺ codoping, the persistent luminescence (delayed lifetime) varied immensely. We demonstrate in Figure 2b that the samples with similar PLQY, Gd₂O₂S:6% Eu³⁺/x% Ti⁴⁺ (1 < x < 9 mol%) led to diversely distinguishable delayed PL lifetimes in the 1.17 ± 0.02 to 5.95 ± 0.07 s range. These delayed lifetimes were determined by isolating a region of interest (ROI) from videos acquired using a 30 fps smartphone camera and fitting a single exponential equation $y = y_0 + A_1 \exp(-t/\tau)$ in a time window selected as described in Figure S6 of the Supporting Information. In brief, the initial boundary time, t₁, was universally taken to be 2 s while the end boundary time, t₂, was the time at which the lifetime extracted from the delayed PL emission video decays to 90%. The reproducibility of the delayed PL lifetime determination by analysis of the smartphone video is shown in Figure S6 and Table S1 of the Supporting Information.

Beyond 9 mol% Ti⁴⁺ codoping, the PLQY starts to decrease with increasing doping leading to a low PLQY value of up to 16% ± 3% for the Gd₂O₂S:6% Eu³⁺/24% Ti⁴⁺ sample. High Ti⁴⁺ codoping also decreases the delayed PL lifetime, with the Gd₂O₂S:6%Eu³⁺/24% Ti⁴⁺ leading to a delayed PL lifetime of 2.90 ± 0.03 s as demonstrated in Figure 2c. Therefore, due to the concentration quenching, both the PLQY (see Figure 2a) and the delayed lifetimes decrease when the Ti⁴⁺ codoping is

more than 9 mol% (Figure 2c,d). A summary of the delayed PL lifetime(s) is presented in Figure 2d. Higher than 9 mol% codoping, thus, only leads to a repeated lifetime (s) with lower PLQY, so are not useful. Therefore, doping the $\text{Gd}_2\text{O}_2\text{S}:6\% \text{Eu}^{3+}$ with up to 9 mol% of Ti^{4+} ions led to a sequence of phosphors with delayed lifetimes varying from 1.17 ± 0.02 to 5.95 ± 0.07 s but with uniform PLQY, providing for two features attractive for persistent PL lifetime based anticounterfeiting applications as discussed here.

In terms of mechanistic understanding, one can conclude that the persistent luminescence in $\text{Gd}_2\text{O}_2\text{S}:6\%\text{Eu}^{3+}/x\%\text{Ti}^{4+}$ emanates from the Eu^{3+} because the emission spectrum of the Ti^{4+} codoped samples is identical to that of the pure Eu^{3+} sample (see Figure 1b). Furthermore, Figure S7 of the Supporting Information illustrates that there is no change of the emission spectrum after the 375 nm excitation is turned off. The emission during excitation and the persistent luminescence has the same spectrum and therefore come from the same state, namely, the $^5\text{D}_0$ state of the Eu^{3+} . Nonetheless, the Ti^{4+} clearly affects the lifetime of the persistent luminescence coming from the Eu^{3+} (Figure 2b,c). The increase of the persistent luminescence lifetime by co-doping with Ti^{4+} has been previously observed.^[24c,36] With special relevance to this work, Lei et al. investigated the persistent luminescence of a wide range of $\text{Gd}_2\text{O}_2\text{S}:\text{RE}^{3+}$, Ti^{4+} , Mg^{2+} materials (RE = Ce, Pr, Nd, Sm, Eu, Tb, Dy, Ho, Er, Tm, Yb).^[32] Whereas the afterglow of most codoped materials had a major component from the Ti emission in their spectrum, the Eu^{3+} material did not.^[32] This motivated us to further develop the $\text{Gd}_2\text{O}_2\text{S}:\text{Eu}^{3+}$, Ti^{4+} material. Our decision was based on a combination of factors. First, the $\text{Gd}_2\text{O}_2\text{S}:\text{Eu}^{3+}$ exhibits an appropriately low-energy CTB for excitation at 375 nm. Second, that the emission only comes from one state in this material means that the lifetime determination from a smartphone video should be easier to realize. If the emission comes from two different states, with different lifetimes, such a determination could be frustrated. Third, given the Ti^{4+} seemed to transfer energy to the Eu, we hypothesized that control over the Ti^{4+} concentration should be an effective way to tune the Eu emission lifetime. Recent detailed work by Luo et al.^[35] gives the best mechanistic insight into the nature of persistent emission in this class of materials. They showed that upon UV excitation, charge transfer excitation can lead to Ti^{3+} or Eu^{2+} along with a hole on the host. In the $\text{Gd}_2\text{O}_2\text{S}$ host, the Eu^{2+} is lower in energy than the Ti^{3+} , so electron transfer from Ti^{3+} to Eu^{2+} will occur. Upon capture of the hole by the Eu^{2+} , the standard delayed emission from Eu^{3+} is observed. This is consistent with the minimal offset in the vacuum referenced binding energies of the Ti^{3+} to Eu^{2+} determined in the literature.^[35] In Figure S8 of the Supporting Information, we show the temperature dependence of the persistent emission lifetime for the $\text{Gd}_2\text{O}_2\text{S}:6\% \text{Eu}^{3+}$ and $\text{Gd}_2\text{O}_2\text{S}:6\% \text{Eu}^{3+}/3\% \text{Ti}^{4+}$ samples. Over the 175 to 350 K temperature range measured, the lifetimes first increase, reach a maximum value at around 250 K, then decrease again. This trend is observed for both samples, and the $\text{Gd}_2\text{O}_2\text{S}:6\% \text{Eu}^{3+}/3\% \text{Ti}^{4+}$ lifetime is roughly a factor of 2 longer than that of the $\text{Gd}_2\text{O}_2\text{S}:6\% \text{Eu}^{3+}$ at all temperatures. This similar trend of the lifetime of the persistent emission with temperature suggests the changes are dominated

by the temperature-dependent position of the CTB relative to the $\text{Eu}^{3+} ^5\text{D}_0$ level, and by the rate of nonradiative deactivation of the CTB. We hypothesize that the extension of the delayed emission of Eu^{3+} by Ti^{4+} in $\text{Gd}_2\text{O}_2\text{S}$ is then due to a delay in the filling of the Eu CTB by the Ti^{4+} slowing the release of the hole on the host (potentially due to charge imbalance effects), and by sometimes necessitating electron transfer between the Ti and Eu before emission. Although further work to solidify the mechanistic understanding is of interest, we certainly demonstrate that the $\text{Gd}_2\text{O}_2\text{S}:\text{Eu}^{3+}/\text{Ti}^{4+}$ is a system that excellently satisfies all the nontrivial requirements for a persistent phosphor with tunable lifetime for smartphone-based lifetime determination.

To demonstrate the applicability of these phosphors for anticounterfeiting, a 4-digit 7-segment display was made by pressing various phosphor powders into pockets machined into a plastic bar as illustrated in Figure 3a. The length and width and depth of a single segment of this display are 10, 3, and 1 mm, respectively. As visually illustrated in Figure 3a, the phosphor powder in segments ① and ② is $\text{Gd}_2\text{O}_2\text{S}:6\%\text{Eu}^{3+}$, the phosphor powder in ③ and ④ is $\text{Gd}_2\text{O}_2\text{S}:6\%\text{Eu}^{3+}/1\%\text{Ti}^{4+}$, and that in segments ⑤, ⑥, and ⑦ is $\text{Gd}_2\text{O}_2\text{S}:6\% \text{Eu}^{3+}/9\% \text{Ti}^{4+}$. We repeated the powder-loading procedure in the four digits shown in Figure 3b. The progression of the afterglow emission after UV excitation is as illustrated in Figure 3b and is described as follows. During UV (375 nm) illumination, and within the 2.5 s following the excitation source being switched off, the luminescent label reads '8 8 8 8'. The display then changes to '3 3 3 3' after the delayed emission of the $\text{Gd}_2\text{O}_2\text{S}:6\%\text{Eu}^{3+}$ (with the shortest lifetime) fades away in the two left-side segments marked ① and ② of each digit. After that, the two lower horizontal segments marked ③ and ④ of each seven-segment digit fade away due to exhaustion of delayed PL luminescence from $\text{Gd}_2\text{O}_2\text{S}:6\%\text{Eu}^{3+}/1\%\text{Ti}^{4+}$, leading the label to read '7 7 7 7'. The '7 7 7 7' displayed segments represent the $\text{Gd}_2\text{O}_2\text{S}:6\%\text{Eu}^{3+}/9\%\text{Ti}^{4+}$ phosphor that has the longest delayed luminescence and is observable even after 10 s.

Like previous work by Liu et al. and Fan et al., the dynamic change of the luminescent label during and after excitation can be examined by eye, providing a further level of anticounterfeiting security compared to a standard luminescent label.^[11b,c] We also note that this holds over a wide variety of temperatures, as the lifetimes of the different phosphors change with temperature in a similar manner (see Figure S9 of the Supporting Information, the times at which the different patterns are visible changes but the same dynamic pattern change occurs).

In a more novel approach that exhibits more quantitative authentication possibilities, the lifetimes here can be verified with the analysis of a smartphone video. Figure 3c indicates that the lifetimes of the phosphors in the segments indicated. These lifetimes are 1.16 ± 0.02 , 3.18 ± 0.04 , and 5.93 ± 0.07 s; and they agree with the calibration lifetimes as plotted in Figure 2d of $\text{Gd}_2\text{O}_2\text{S}:6\%\text{Eu}^{3+}$, $\text{Gd}_2\text{O}_2\text{S}:6\%\text{Eu}^{3+}/1\% \text{Ti}^{4+}$ and $\text{Gd}_2\text{O}_2\text{S}:6\%\text{Eu}^{3+}/9\% \text{Ti}^{4+}$, respectively. Thus, with safe and inexpensive 375 nm LED excitation and smartphone camera detection, a quantitative analysis of our anticounterfeiting labels is realizable in the over-the-counter sale of labeled products. In a broader context, this would allow the use of smartphones to decode the delayed PL lifetimes of ROIs of the patterns at the

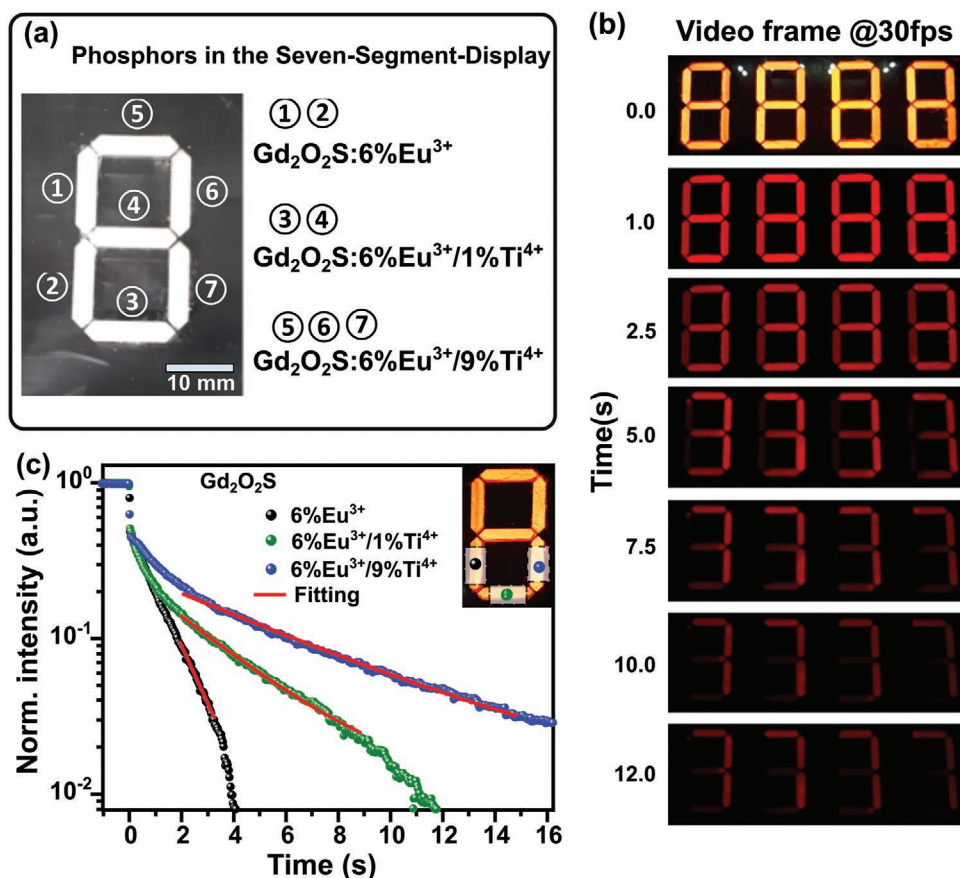


Figure 3. a) Information indicating the specific phosphors pressed on each of the seven-segment four-digit display. b) Video frames of interest extracted from smartphone-acquired videos of $\text{Gd}_2\text{O}_2\text{S}:6\%\text{Eu}^{3+}/x\%\text{Ti}^{4+}$ for ($x = 0, 1,$ and 9 mol%) demonstrating dynamic luminescence for anticounterfeiting applications in a seven-segment four-digit display filled with the phosphors. Upon UV excitation, “8 8 8 8” is displayed. This changes to “3 3 3 3” after the delayed luminescence of $\text{Gd}_2\text{O}_2\text{S}:6\%\text{Eu}^{3+}$ is completely exhausted after ≈ 5 s. The display later transitions to “7 7 7 7” when the $\text{Gd}_2\text{O}_2\text{S}:6\%\text{Eu}^{3+}/1\%\text{Ti}^{4+}$ exhausts its luminescence. The final displayed “7 7 7 7” comes from the delayed luminescence of the $\text{Gd}_2\text{O}_2\text{S}:6\%\text{Eu}^{3+}/9\%\text{Ti}^{4+}$ that has the longest delayed luminescence that is the only one observed after 10 s. c) Delayed PL lifetime of the three phosphors as extracted from the first digit in segments ②, ③, and ⑦ as mapped in the inset figure with the legend colors after excitation with UV (375 nm) LED.

point of sale to confirm the authenticity. Alternatively, a subset of the lifetimes of the anticounterfeiting image could be read out by a structured illumination selecting individual regions (see Figure S10, Supporting Information).

For practical mass application, one can realize these patterns via printing. Although inkjet printing is challenging with micrometer-sized particles (and long term either smaller particles or other printing techniques should be used), for an initial demonstration we ink-jet print the phosphors as schematically illustrated in Figure 4a. For this demonstration, a pattern containing the concealed information “I M T” was printed using a Dimatix DMP-2831 inkjet printer in which the first cartridge printed the “I M T” patterned-dots with the $\text{Gd}_2\text{O}_2\text{S}:6\%\text{Eu}^{3+}/9\%\text{Ti}^{4+}$ based ink. The second cartridge, containing the $\text{Gd}_2\text{O}_2\text{S}:6\%\text{Eu}^{3+}/3\%\text{Ti}^{4+}$ printed the rest of the composite pattern. While the patterns are seen as a batch of white dots in the absence of UV light, shining UV light at them first reveals red-emitting phosphor dots. When the excitation source is removed, the pattern formed by $\text{Gd}_2\text{O}_2\text{S}:6\%\text{Eu}^{3+}/3\%\text{Ti}^{4+}$ decays faster than the $\text{Gd}_2\text{O}_2\text{S}:6\%\text{Eu}^{3+}/9\%\text{Ti}^{4+}$ based patterns

revealing the “I M T” pattern as shown by the frame progression in Figure 4b. A binary image is also shown in Figure 4b revealing the “I M T” pattern and thus providing for alternative authentication via image binarization. A zoom-in to the video frames further reveals that it is possible to integrate this smartphone-based temporal anticounterfeiting with other anticounterfeiting technologies like the ones relying on physically unclonable functions (PUF).^[6a] The PUFs provide for a unique unclonable approach that is mass-producible and convenient in the authentication.

This demonstration indicates the power of time-based dynamic anticounterfeiting in which the patterns in display change post excitation. In two previous examples (see Figures 3 and 4), we demonstrated one method by which these phosphors can provide overt and covert anticounterfeiting characteristics; namely, changes in a pattern visible by the eye, and determination of the decay lifetime of certain parts of the pattern through the analysis of a smartphone video. In Figure 5, we demonstrate another method to realize an anticounterfeiting label using these phosphors. Here, two pairs of two

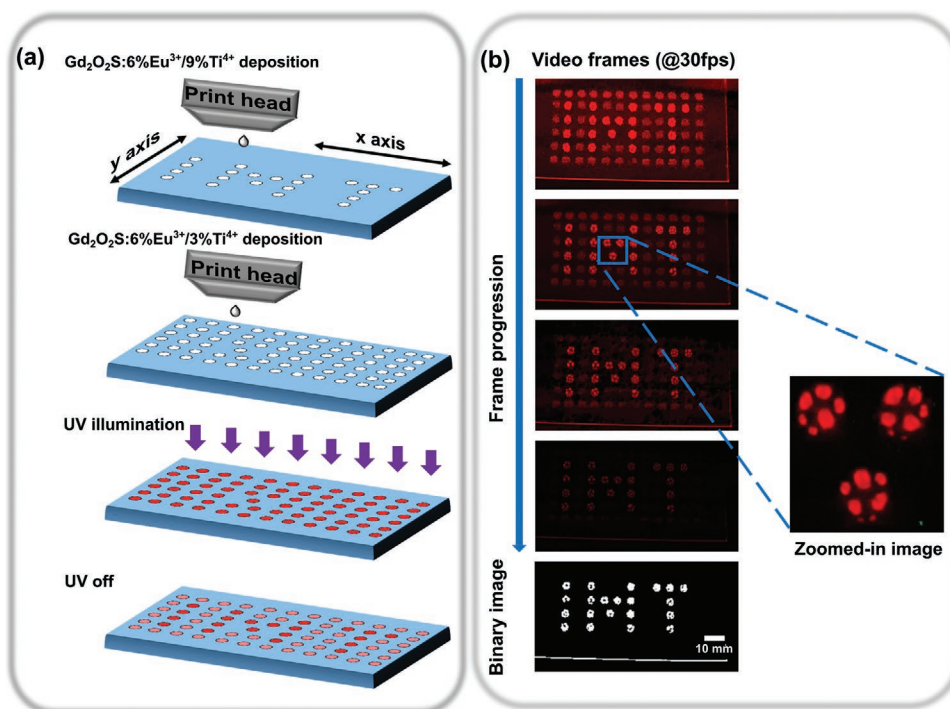


Figure 4. a) Schematic of the process of inkjet-printing “I M T” patterns using $\text{Gd}_2\text{O}_2\text{S}:6\%\text{Eu}^{3+}/9\%\text{Ti}^{4+}$ and $\text{Gd}_2\text{O}_2\text{S}:6\%\text{Eu}^{3+}/3\%\text{Ti}^{4+}$. b) Frames of video progression of the label after UV illumination showing initial brightness of the prints followed by subsequent different rate PL lifetime decay that reveals the “I M T” label. A binary image visualizing the “I M T” logo representing the $\text{Gd}_2\text{O}_2\text{S}:6\%\text{Eu}^{3+}/9\%\text{Ti}^{4+}$ phosphor. The zoomed-in image shows the possibility of having unique physical architectures (cat-like-footprints) for enhanced physical masking.

phosphors that exhibit similar, short decay times (1.41 ± 0.02 and 1.65 ± 0.02 s; or 1.27 ± 0.02 , and 1.41 ± 0.02 s, respectively) were chosen to make patterns as pictured in Figure 5a. We developed the patterns shown in Figure 5b by drop-casting dots of the phosphor suspension onto a glass substrate maintained at 65°C . The elevated temperature allowed faster drying of the dropped suspension, hence, minimizing the spread-radius. Here the covert pattern is either concealed in a phosphor with a slightly longer (label “B”), or shorter (label “C”) lifetime than the surrounding obfuscation pattern. The time-evolution of the pattern can be made difficult to resolve by the eye. Whereas it is possible to make out the concealed pattern by careful examination by the eye of label “B,” it is difficult to detect the concealed pattern in label C by eye (Figure 5b). It is challenging to distinguish the label “A” and label “C” by direct eye observation. However, a simple analysis of still frames from a smartphone video is sufficient to reveal the concealed pattern. In the case of label B (Figure 5b), the binarization of the still image after 4 s with an appropriate threshold directly reveals the concealed pattern. For label C, such a binarization creates a mask that is then applied to the still image during excitation to reveal the concealed pattern. Therefore, the short but tunable lifetimes of these phosphors can also be exploited for anticounterfeiting techniques in which the dynamic change of a pattern is unobservable by the eye but can be verified by a previously defined comparison of still images extracted from a smartphone video.

3. Conclusion

In summary, we demonstrate that the lifetime of the delayed emission in $\text{Gd}_2\text{O}_2\text{S}:6\%\text{Eu}^{3+}/x\%\text{Ti}^{4+}$ can be tuned from 1.17 ± 0.02 to 5.95 ± 0.07 s for Ti^{4+} codoping concentrations from 0 to 9%. Over this Ti^{4+} codoping range the PLQY of the phosphors remained over 46%. This phosphor’s delayed PL lifetime palette, which maintains good emission efficiency while allowing the persistent lifetime to be gradually tuned, is attractive for anticounterfeiting applications. Using patterns based on phosphors with a more significant persistent lifetime difference, dynamic pattern changes of the luminescence are visible by the eye after the 375 nm LED excitation is switched off. This anticounterfeiting feature was strengthened using a smartphone video to determine the persistent lifetimes at specific areas of the pattern and authenticate these against known reference values. Furthermore, dynamic images based on materials with similar (and short) delayed lifetimes can be made difficult to resolve by eye, but easily authenticated with an appropriate analysis of still frames extracted from a smartphone video. This novel direction of developing persistent phosphors whose lifetimes are controllably tunable in the “sweet spot” for lifetime determination with a smartphone camera, i.e., in the range of 100 ms to 10 s, is attractive in terms of implementing an anticounterfeiting technology. Based on these phosphors, in addition to overt dynamic features verifiable by eye, covert features that are authenticated

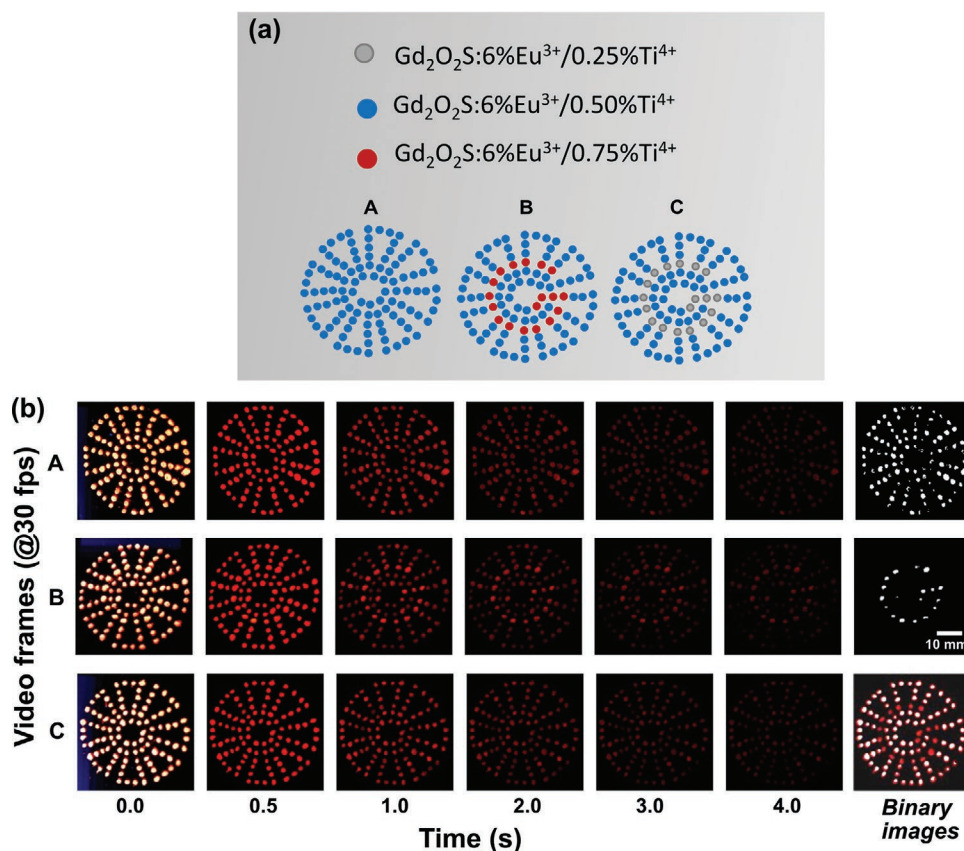


Figure 5. Anticounterfeiting label based on analysis of still images from a smartphone video. a) Schematic of the three label patterns created, and the phosphors contained in patterns. b) Frames extracted from smartphone videos of each label, the hidden image is obtained by making a binary image with an appropriate threshold from the 4 s image (label “B”), or using such a binary image to mask the image collected at 0.5 s (label “C”).

based on smartphone video analysis such as precise lifetimes, or dynamic changes based on lifetimes too similar to differentiate by eye can be included. These results inspire further work to focus on expanding the usage of smartphones coupled with phosphors engineered to have appropriately delayed luminescence lifetimes for robust quantitative authentication of luminescent anticounterfeiting labels.

4. Experimental Section

Synthesis of $\text{Gd}_2\text{O}_2\text{S}:\text{Eu}^{3+}/\text{Ti}^{4+}$: The $\text{Gd}_{0.94-x}\text{Eu}_{0.06}\text{Ti}_x)_2\text{O}_2\text{S}$ for ($x = 0$ to 24 mol%) were synthesized by a flux-assisted solid-state reaction in a furnace system according to procedures published in the literature.^[37] The starting materials were Gd_2O_3 (ChemPur, 99.9%), Eu_2O_3 (ChemPur, 99.9%), and sulfur (S) (ChemPur, 99+ %), with Na_2CO_3 (ChemPur, 99+ %) and K_2CO_3 (ChemPur, 99+ %), used as flux. The molar ratio of the fluxing agents $\text{Na}_2\text{CO}_3:\text{K}_2\text{CO}_3$ was set at 2:3, respectively, and excess sulfur was used to ensure complete sulfurization.

Photoluminescence Quantum Yield: The absolute PLQY was determined using the de Mello method.^[38] This was recorded using an integrated system encompassing a spectrometer (AvaSpec-HS2048XL, Avantes) attached to an integrating sphere (15 cm diameter, Labsphere) and a UV LED ($\lambda = 375$ nm) excitation source controlled with a bench-top laser diode controller (ITC4001, Thorlabs). The powder samples, in quartz cuvettes, were placed inside the integrating sphere,

with the UV LED directed to them via the sphere side opening. Another opening in the integrating sphere was connected to an optical fiber of 1 mm diameter (FP100URT, Thorlabs) for collecting the signal. This opening had a baffle immediately before the fiber for preventing direct illumination of the fiber and consequently, the detector from the UV LED and sample emissions. Measurements of the empty sphere, direct and indirect excitation spectra, direct and indirect emission spectra, and black background were recorded, from which the PLQY was calculated.

Inkjet Printing: The printing was conducted using a Dimatix DMP-2831 inkjet printer equipped with a 10 pl cartridge (21 μm nozzle). The printer jetting frequency of 5 kHz was kept and the drop spacing at 20 μm was set. A custom-designed waveform was developed for each ink. The temperatures of the print head and the glass substrate were set to 40 and 28 $^\circ\text{C}$, respectively.

Glass substrates (Borofloat Schott) were cleaned in an ultrasonic bath while submerged in deionized water, acetone, and isopropanol for 10 min each time. The substrates were then treated under argon plasma for 1 min. The employed inks consisted of a 20 mg mL^{-1} solution of the phosphor material ($\text{Gd}_2\text{O}_2\text{S}:6\%\text{Eu}^{3+}/3\%\text{Ti}^{4+}$ or $\text{Gd}_2\text{O}_2\text{S}:6\%\text{Eu}^{3+}/9\%\text{Ti}^{4+}$) in Terpineol. The solutions were filtered with 10, 5, and then 2.7 μm syringe filters. Before the deposition, the ink-solutions were ultrasonicated for 1 h to reduce particle agglomeration. An SEM image of the particles left by a small drop of the ink is presented in Figure S3 of the Supporting Information. The pattern deposition process then involved first printing the $\text{Gd}_2\text{O}_2\text{S}:6\%\text{Eu}^{3+}/9\%\text{Ti}^{4+}$ based ink to form the “I M T” pattern and then $\text{Gd}_2\text{O}_2\text{S}:6\%\text{Eu}^{3+}/3\%\text{Ti}^{4+}$ ink dispersion to form a composite print. After deposition, the samples were dried at 120 $^\circ\text{C}$ for 5 min. All the printing process occurred in cleanroom conditions (RH = 50%, RT = 20 $^\circ\text{C}$).

Drop Casting: The suspensions of phosphors were created by dissolving 5%w/w of polyvinylpyrrolidone in ethanol and adding 95%w/w phosphor materials while stirring for 15 min. To cast the suspensions into a pattern on the cleaned glass slide, the slides were maintained at 60 °C as the patterns were copy-casted in the glass. This was achieved by having a follow-up pattern under the glass slide for which the suspensions were drop-casted.

PL Lifetime Experiments: The samples were placed inside small ceramic crucibles and illuminated with a UV LED (375 nm, adjusted to 25 mW cm⁻² intensity at the sample) in the dark at a frequency of 0.017 Hz with a duty cycle of 17%. The emission was then video recorded using a 16-megapixel smartphone camera (Galaxy A5 (2017), Samsung electronics). The smartphone camera settings were controlled using a third-party application (Mark Harman, camera HD, Open Camera V1.0, Code 1 © 2013–2016) found in the Galaxy store also named Open Camera (v1.48.1 Code: 77) in Google Play. The camera app settings were first set to manual mode via the application programming interface (API) by changing it to Camera 2API from the default Camera API. In this mode, the settings were then adjusted as follows. The ISO was set to 1350, the spatial resolution to 1980 × 1080 pixels, the frame rate set to 30 fps, while balance set to fluorescent, color effect to none. The autolevel was then unchecked and the shutter speed was set to 1/30 s. These settings were then saved and used for all video acquisitions. The stability of the lifetime under UV exposure was also explored (Figure S11, Supporting Information).

Supporting Information

Supporting Information is available from the Wiley Online Library or from the author.

Acknowledgements

The authors gratefully acknowledge financial support by the Helmholtz Association: the Recruitment Initiative of B.S.R., the Helmholtz Energy Materials Foundry (HEMF), and Research Field Energy – Program Materials and Technologies for the Energy Transition – Topic 1 Photovoltaics. N.K. and V.K. thank the German Academic Exchange Service, DAAD, for financial support and Karlsruhe School of Optics and Photonics (KSOP) for training. G.H.S. and L.A.R.P. acknowledge funding by the German Federal Ministry for Research and Education (BMBF) through the project FKZ: 03INT606AG.

Open access funding enabled and organized by the project DEAL.

Conflict of Interest

The authors declare no conflict of interest.

Data Availability Statement

Research data are not shared.

Keywords

anticounterfeiting, delayed luminescence, dynamic, fluorescence, smartphone

Received: January 15, 2021
Revised: March 3, 2021
Published online: May 28, 2021

- [1] a) F. Economics, *Report prepared for BASCAP and INTA*, Recuperado de https://www.inta.org/communications/documents/2017_frontier_report.pdf 2017 (accessed: October 2020); b) M. Kazimierzczak, OECD, E. U. I. P. Office, *Trade in Counterfeit and Pirated Goods*, OECD Publishing 2016.
- [2] a) Z. C. Kennedy, D. E. Stephenson, J. F. Christ, T. R. Pope, B. W. Arey, C. A. Barrett, M. G. Warner, *J. Mater. Chem. C* 2017, 5, 9570; b) J. F. Ramalho, S. F. Correia, L. Fu, L. L. António, C. D. Brites, P. S. André, R. A. Ferreira, L. D. Carlos, *Adv. Sci.* 2019, 6, 1900950.
- [3] Y. Cui, R. S. Hegde, I. Y. Phang, H. K. Lee, X. Y. Ling, *Nanoscale* 2014, 6, 282.
- [4] a) H. Hu, Q.-W. Chen, J. Tang, X.-Y. Hu, X.-H. Zhou, *J. Mater. Chem.* 2012, 22, 11048; b) H. Hu, H. Zhong, C. Chen, Q. Chen, *J. Mater. Chem. C* 2014, 2, 3695.
- [5] a) K. L. Włodarczyk, M. Ardrón, N. J. Weston, D. P. Hand, *J. Mater. Process. Technol.* 2019, 264, 328; b) G. Ruffato, R. Rossi, M. Massari, E. Mafakheri, P. Capaldo, F. Romanato, *Sci. Rep.* 2017, 7, 18011.
- [6] a) Y. Liu, F. Han, F. Li, Y. Zhao, M. Chen, Z. Xu, X. Zheng, H. Hu, J. Yao, T. Guo, *Nat. Commun.* 2019, 10, 2409; b) X. Hou, C. Ke, C. J. Bruns, P. R. McGonigal, R. B. Pettman, J. F. Stoddart, *Nat. Commun.* 2015, 6, 6884; c) M. R. Carro-Temboury, R. Arppe, T. Vosch, T. J. Sørensen, *Sci. Adv.* 2018, 4, 1701384; d) T. Ma, T. Li, L. Zhou, X. Ma, J. Yin, X. Jiang, *Nat. Commun.* 2018, 11, 1811.
- [7] a) J. Andres, R. D. Hersch, J. E. Moser, A. S. Chauvin, *Adv. Funct. Mater.* 2014, 24, 5029; b) X. Yang, L. Zhao, W. Zeng, Z. Liu, X. Fan, S. Tian, H. Zhang, X. Xu, J. Qiu, X. Yu, *J. Am. Ceram. Soc.* 2020, 103, 2235.
- [8] H. Zhao, X. Qin, L. Zhao, S. Dong, L. Gu, W. Sun, D. Wang, Y. Zheng, *ACS Appl. Mater. Interfaces* 2020, 12, 8952.
- [9] a) L. Bai, N. Xue, Y. Zhao, X. Wang, C. Lu, W. Shi, *Nano Res.* 2018, 11, 2034; b) J. Song, Q. Ma, Y. Liu, Y. Guo, F. Feng, S. Shuang, *RSC Adv.* 2019, 9, 38568; c) Y. Liu, K. Ai, L. Lu, *Nanoscale* 2011, 3, 4804; d) P. Kumar, K. Nagpal, B. K. Gupta, *ACS Appl. Mater. Interfaces* 2017, 9, 14301; e) L. Ji, J. Zhou, J. Zhang, Z. Zhang, Z. Ma, W. Wang, H. Li, C. Wu, *J. Am. Ceram. Soc.* 2019, 102, 5465.
- [10] C. Shi, X. Shen, Y. Zhu, X. Li, Z. Pang, M. Ge, *ACS Appl. Mater. Interfaces* 2019, 11, 18548.
- [11] a) J. Wang, J. Ma, J. Zhang, Y. Fan, W. Wang, J. Sang, Z. Ma, H. Li, *ACS Appl. Mater. Interfaces* 2019, 11, 35871; b) Y. Fan, X. Jin, M. Wang, Y. Gu, J. Zhou, J. Zhang, Z. Wang, *Chem. Eng. J.* 2020, 393, 124799; c) Z. Liu, L. Zhao, W. Chen, X. Fan, X. Yang, S. Tian, X. Yu, J. Qiu, X. Xu, *J. Mater. Chem. C* 2018, 6, 11137.
- [12] a) X. Han, E. Song, B. Zhou, Q. Zhang, *J. Mater. Chem. C* 2019, 7, 8226; b) S. K. B. Mane, Y. Mu, E. Ubba, Z. Yang, J. Zhao, Z. Chi, *J. Mater. Chem. C* 2019, 7, 15219; c) J. Chen, T. Yu, E. Ubba, Z. Xie, Z. Yang, Y. Zhang, S. Liu, J. Xu, M. P. Aldred, Z. Chi, *Adv. Opt. Mater.* 2019, 7, 1801593; d) Y. Lu, J. Zhao, R. Zhang, Y. Liu, D. Liu, E. M. Goldys, X. Yang, P. Xi, A. Sunna, J. Lu, *Nat. Photonics* 2014, 8, 32; e) M. Tan, F. Li, X. Wang, R. Fan, G. Chen, *ACS Nano* 2020, 14, 6532.
- [13] H. Sun, S. Liu, W. Lin, K. Y. Zhang, W. Lv, X. Huang, F. Huo, H. Yang, G. Jenkins, Q. Zhao, W. Huang, *Nat. Commun.* 2014, 5, 3601.
- [14] S. Kalytchuk, Y. Wang, K. i. Poláková, R. Zbořil, *ACS Appl. Mater. Interfaces* 2018, 10, 29902.
- [15] L. Ding, X.-d. Wang, *J. Am. Chem. Soc.* 2020, 142, 13558.
- [16] a) Y. Li, M. Gecevicius, J. Qiu, *Chem. Soc. Rev.* 2016, 45, 2090; b) D. Poelman, D. Van der Heggen, J. Du, E. Cosaert, P. F. Smet, *J. Appl. Phys.* 2020, 128, 240903.
- [17] P. Pei, P. Duanmu, B. Wang, X. Miao, C. Zhang, W. Liu, *Dalton Trans.* 2021, 50, 3193.
- [18] Z. Long, Y. Wen, J. Zhou, J. Qiu, H. Wu, X. Xu, X. Yu, D. Zhou, J. Yu, Q. Wang, *Adv. Opt. Mater.* 2019, 7, 1900006.
- [19] J. Sang, J. Zhou, J. Zhang, H. Zhou, H. Li, Z. Ci, S. Peng, Z. Wang, *ACS Appl. Mater. Interfaces* 2019, 11, 20150.

- [20] a) W. Zhao, Z. He, B. Z. Tang, *Nat. Rev. Mater.* **2020**, *5*, 869; b) X. Yang, D. Yan, *Adv. Opt. Mater.* **2016**, *4*, 897.
- [21] a) R. Kabe, C. Adachi, *Nature* **2017**, *550*, 384; b) W. Li, Z. Li, C. Si, M. Y. Wong, K. Jinnai, A. K. Gupta, R. Kabe, C. Adachi, W. Huang, E. Zysman-Colman, *Adv. Mater.* **2020**, *32*, 2003911; c) N. Nishimura, Z. Lin, K. Jinnai, R. Kabe, C. Adachi, *Adv. Funct. Mater.* **2020**, *30*, 2070138; d) Y. Zhang, T. S. Lee, J. M. Favale, D. C. Leary, J. L. Petersen, G. D. Scholes, F. N. Castellano, C. Milsmann, *Nat. Chem.* **2020**, *12*, 345.
- [22] a) Y. Sun, S. Liu, L. Sun, S. Wu, G. Hu, X. Pang, A. T. Smith, C. Hu, S. Zeng, W. Wang, *Nat. Commun.* **2020**, *11*, 5591; b) K. Jiang, L. Zhang, J. Lu, C. Xu, C. Cai, H. Lin, *Angew. Chem.* **2016**, *128*, 7347.
- [23] N. Katumo, G. Gao, F. Laufer, B. S. Richards, I. A. Howard, *Adv. Opt. Mater.* **2020**, *8*, 2000507.
- [24] a) Q. Guanming, W. Hui, C. Yongjie, G. Xiujuan, Y. Ying, S. Shuang, S. Zhaoxin, *J. Rare Earths* **2007**, *25*, 104; b) J. Miranda de Carvalho, C. C. S. Pedroso, I. P. Machado, J. Hölsä, L. C. V. Rodrigues, P. Głuchowski, M. Lastusaari, H. F. Brito, *J. Mater. Chem. C* **2018**, *6*, 8897; c) Z. Hong, P. Zhang, X. Fan, M. Wang, *J. Lumin.* **2007**, *124*, 127.
- [25] J. Zhang, Z. Zhang, T. Wang, W. Hao, *Mater. Lett.* **2003**, *57*, 4315.
- [26] Y. Lin, Z. Tang, Z. Zhang, C. W. Nan, *J. Alloys Compd.* **2003**, *348*, 76.
- [27] M. Kneissl, T.-Y. Seong, J. Han, H. Amano, *Nat. Photonics* **2019**, *13*, 233.
- [28] F. Behar-Cohen, G. Baillet, T. de Agyuavives, P. O. Garcia, J. Krutmann, P. Peña-García, C. Reme, J. S. Wolffsohn, *Clin. Ophthalmol.* **2014**, *8*, 87.
- [29] a) K. Binnemans, *Coord. Chem. Rev.* **2015**, *295*, 1; b) S. A. Osseni, S. Lechevallier, M. Verelst, P. Perriat, J. Dexpert-Ghys, D. Neumeyer, R. Garcia, F. Mayer, K. Djanashvili, J. A. Peters, *Nanoscale* **2014**, *6*, 555; c) P. Rodnyí, *Opt. Spectrosc.* **2009**, *107*, 270.
- [30] Z. Q. Zheng, X. P. Zhou, *J. Am. Ceram. Soc.* **2013**, *96*, 3504.
- [31] S. Som, A. Choubey, S. Sharma, *J. Exp. Nanosci.* **2015**, *10*, 350.
- [32] B. Lei, Y. Liu, J. Zhang, J. Meng, S. Man, S. Tan, *J. Alloys Compd.* **2010**, *495*, 247.
- [33] a) Y. Tang, S. Dai, Y. Fang, *J. Appl. Phys.* **2009**, *105*, 033101; b) H. Bettentrup, K. Eskola, J. Hölsä, A. Kotlov, M. Lastusaari, M. Malkamäki, "Luminescence properties of Eu³⁺ and TiIV/ZrIV doped yttrium oxysulfides (Y₂O₂S:Eu³⁺, TiIV/ZrIV)", presented at *IOP Conf. Series: Materials Science and Engineering*, University of Pécs, Hungary, July **2010**.
- [34] J. Hölsä, T. Laamanen, M. Lastusaari, M. Malkamäki, J. Niittykoski, E. Zych, *Opt. Mater.* **2009**, *31*, 1791.
- [35] H. Luo, A. J. Bos, P. Dorenbos, *J. Phys. Chem. C* **2017**, *121*, 8760.
- [36] a) X. Zhou, M. Xing, T. Jiang, Y. Fu, Y. Peng, H. Wang, X. Luo, *J. Alloys Compd.* **2014**, *585*, 376; b) Z. Hong, P. Zhang, Q. Huang, X. Fan, M. Wang, *J. Inorg. Mater.* **2006**, *21*, 329; c) P. Zhang, Z. Hong, M. Wang, X. Fang, G. Qian, Z. Wang, *J. Lumin.* **2005**, *113*, 89; d) Y. Iida, K. Sawamura, K. Iwasaki, T. Nakanishi, F. Iwakura, Y. Nakajima, A. Yasumori, *Sens. Mater.* **2020**, *32*, 1427.
- [37] F. Wang, X. Chen, D. Liu, B. Yang, Y. Dai, *J. Mol. Struct.* **2012**, *1020*, 153.
- [38] J. C. de Mello, H. F. Wittmann, R. H. Friend, *Adv. Mater.* **1997**, *9*, 230.